https://doi.org/10.5194/egusphere-2026-2350
Preprint. Discussion started: 8 May 2026

Atmospheric deserts and extreme weather events: co-occurrence with positive temperature anomalies, thunderstorms, and dust

Fiona Fix-Hewitt[1], Achim Zeileis[2], Isabell Stucke[1], Reto Stauffer[3], and Georg J. Mayr[1]

[1]Department of Atmospheric and Cryospheric Sciences, Universität Innsbruck, Innsbruck, Austria
[2]Department of Statistics, Universität Innsbruck, Innsbruck, Austria
[3]Department of Statistics & Digital Science Center, Universität Innsbruck, Innsbruck, Austria

Correspondence: Fiona Fix-Hewitt (fiona.fix@uibk.ac.at)

Abstract.

Elevated mixed layers are known to influence near-surface temperatures and the formation of thunderstorms. Here we investigate the generalisation of elevated mixed layers, so called "atmospheric deserts": air masses originating in hot, dry, deep, convective boundary layers over arid and/or elevated regions. Atmospheric deserts are frequently advected over Europe and can modify temperature profiles throughout the free troposphere, with implications for convective potential. We therefore investigate their co-occurrence with positive temperature anomalies and thunderstorms over Europe. We also investigate their co-occurrence with dust events, since the source region for atmospheric deserts over Europe is also the main source region for dust events.

For this purpose, atmospheric desert air is tracked during the study period from May 2022 to April 2024, using a direct detection method based on Lagrangian trajectories initiated at a very high spatio-temporal resolution.

Positive temperature anomaly events, thunderstorms, and dust events are identified from ERA5 atmospheric reanalysis, lightning data from Blitzortung.org, and EAC4 atmospheric composition reanalysis, respectively. Conditional probabilities and corresponding odds ratios provide insight into whether the mentioned extreme events occur more frequently in the presence of atmospheric deserts.

The probability of events with positive temperature anomalies, thunderstorms, or dust anomalies is enhanced in the presence of atmospheric deserts in almost the entire domain. In most of the domain, positive temperature anomaly events are more likely given the presence of atmospheric desert air, but trapping of heat under a cap could not be confirmed as the main driver. Lightning probability is clearly enhanced along the atmospheric desert edges, and, in contrast to expectations, also in the atmospheric desert centres. In western Europe, up to 50% of occurrences of atmospheric desert air are accompanied by unusually high amounts of dust. Dust events co-occur almost exclusively with atmospheric deserts.

1 Introduction

Atmospheric deserts (ADs; Fix et al., 2024; Fix-Hewitt et al., 2026) are air masses that originate in the hot, dry, deep convective boundary layers (CBLs) of desert and arid regions. While they are advected over thousands of kilometres, they can be gradually modified by diabatic processes and differential advection. They are therefore a generalisation of elevated mixed layers (EMLs;

https://doi.org/10.5194/egusphere-2026-2350
Preprint. Discussion started: 8 May 2026

e.g. Carlson and Ludlam, 1968) which retain their neutral stratification while being advected from the CBL of (elevated) arid regions over cooler, moister low-level air. Our direct detection approach via Lagrangian tracking allows the investigation of ADs for the first time, as it does not require recognisable features in the vertical profiles of the target regions.

ADs have been shown to occur frequently in Europe and affect large parts of the European domain (Fix-Hewitt et al., 2026). EMLs have been shown to influence thunderstorm and heat wave formation (e.g. Carlson and Ludlam, 1968; Carlson et al., 1980, 1983; Keyser and Carlson, 1984; Farrell and Carlson, 1989; Lanicci and Warner, 1991b; Arritt et al., 1992; Johns and Dorr, 1996; Banacos and Ekster, 2010; Lewis and Gray, 2010; Sibley, 2012; Peyraud, 2013; Dahl and Fischer, 2016; Cordeira et al., 2017; Ribeiro and Bosart, 2018; Li et al., 2021; de Villiers, 2020; Feldmann et al., 2021; Wilkinson and Neal, 2021; Young and Grahame, 2023; Andrews et al., 2024; Schultz et al., 2025a, b). In an AD case study in mid June 2022 (Fix et al., 2024) lightning occurred close to the AD edge at 800 hPa, and high near-surface temperatures were recorded in the AD's centre. Therefore, in this work we want to address the question whether ADs show a similar behaviour as EMLs and co-occur with positive temperature anomalies (PTAs), and whether thunderstorm formation is favoured in specific regions of the ADs. Additionally, the source region of ADs in Europe is North Africa, which contains the largest and most persistently active dust sources (Prospero et al., 2021), so we want to investigate how often ADs and strong dust events co-occur.

This article is structured as follows: Necessary background on ADs, EMLs, and dust events is given in Sect. 2. The data and methods used to investigate the co-occurrence of ADs with positive temperature anomalies, thunderstorms and dust events are presented in Sections 3 and 4. This includes the datasets, as well as the Lagrangian detection method, and statistical tools. Results for the co-occurrence of ADs with positive temperature anomalies, thunderstorms, and dust are shown and discussed in Sections 5.1, 5.2, and 5.3, respectively. A summary is presented in Section 6.

2 Background

ADs over Europe are frequent (up to 60% of the time in some regions), albeit short-lived (persistence of approximately one day duration on average), and can cover large parts of Europe (up to 72% of the land-area, results based on May 2022 - April 2024, 30° W to 60° E and 37 to 73°; Fix-Hewitt et al., 2026). Synoptic patterns related to AD events were found to be characterised by either a trough extending far south, or a ridge extending far north, leading to east- or north-eastward transport of air from the source to the target region (Fix-Hewitt et al., 2026). Different air streams emerge, some of which experience an increase in potential temperature (e.g. through condensation), while others experience a decrease (through evaporation, mixing, radiative cooling; Fix-Hewitt et al., 2026). One air stream almost conserves its thermodynamic properties, which makes it EML like.

As warm and dry air masses EMLs are advected over cooler and moister local air masses. They then form an elevated, well-mixed layer with high potential temperature, which often leads to a layer of very strong stability – a "cap" or even capping inversion – immediately atop the local boundary layer (BL; e.g. Carlson and Ludlam, 1968; Carlson et al., 1983; Farrell and Carlson, 1989; Lanicci and Warner, 1991a; Andrews et al., 2024). Strong capping can confine small-scale convection to a shallow layer and hinder the growth and mixing of the local boundary layer, which leads to heat accumulation underneath

https://doi.org/10.5194/egusphere-2026-2350
Preprint. Discussion started: 8 May 2026

(Cordeira et al., 2017). The results are high near surface temperatures, higher wet bulb temperatures and increased instability (Carlson and Ludlam, 1968; Carlson et al., 1983; Cordeira et al., 2017, and others).

In spite of the resulting increased convective available potential energy (CAPE), thunderstorms are unlikely to erupt in the centre of EMLs, where convective inhibition (CIN) is large due to the stable stratification above the BL (e.g. Carlson et al., 1980, 1983; Banacos and Ekster, 2010; Cordeira et al., 2017; Ribeiro and Bosart, 2018). Near the edges, however, the cap (and CIN) tends to be weaker and its base height higher, so that thunderstorms can erupt. Various processes have been suggested to erode the cap and trigger convection near the EML edges, for example underrunning of the moist air from below (Carlson et al., 1983; Farrell and Carlson, 1989; Johns and Dorr, 1996), and ageostrophic circulations at the midlevel baroclinic zone or a convergence line near the edge (Keyser and Carlson, 1984; Dahl and Fischer, 2016). The consequence is that especially severe storms are observed near the EML egde (Carlson and Ludlam, 1968; Carlson et al., 1980, 1983; Keyser and Carlson, 1984; Farrell and Carlson, 1989; Lanicci and Warner, 1991b; Arritt et al., 1992; Johns and Dorr, 1996; Banacos and Ekster, 2010; Lewis and Gray, 2010; Dahl and Fischer, 2016; Ribeiro and Bosart, 2018; Li et al., 2021; Wilkinson and Neal, 2021; Andrews et al., 2024, and others). A similar behaviour was also observed by Fix et al. (2024) in the more general case of an AD.

Furthermore, ADs bring air from northern Africa to Europe. Since northern Africa contains the largest and most active dust sources in the world (Prospero et al., 2021), ADs can transport dust to the target region, per definition. However, whether these air masses actually carry significant dust depends on mobilisation processes in the source region, which depend on wind and soil properties (e.g. Knippertz, 2014; Barkan et al., 2005). Understanding the prevalence of dust is crucial, as it can impact air quality, influence temperature at various altitudes via direct, semi-direct and indirect effects (Penner et al., 2001; Helmert et al., 2007; Bangert et al., 2012). Dust can also influence cloud formation, acting as condensation nuclei, which can lead to "dusty cirrus" clouds, which pose challenges especially in weather forecast modelling (Seifert et al., 2023; Hermes et al., 2024). In this study we focus on how often ADs are also accompanied by strong dust anomalies.

3 Data

We analyse the 2-year period from 01 May 2022, 00 UTC to 30 April 2024, 23 UTC. To investigate the co-occurrence of ADs and positive temperature anomalies (PTAs), dust, and thunderstorms, we employ an atmospheric reanalysis dataset (ERA5, Sect. 3.1; Hersbach et al., 2020), a reanalysis of the atmospheric composition (EAC4, Sect. 3.3; Inness et al., 2019), and lightning data (Blitzortung.org, Sect 3.2; Wanke et al., 2014).

3.1 Atmopsheric reanalyis

The latest global reanalysis, ERA5, from the European Centre for Medium Range Weather Forecasts (ECMWF; Hersbach et al., 2020), is used in this study. The model configuration corresponds to IFS Cy41r2 with a 0.25° horizontal resolution. The data are provided hourly on 137 vertical model levels extending up to 1 Pa (Hersbach et al., 2020). Consequently, the vertical spacing is approximately 20 m near the surface and around 300 m at 500 hPa. In this work, ERA5 single-level and

https://doi.org/10.5194/egusphere-2026-2350
Preprint. Discussion started: 8 May 2026

model-level fields on the lowest 74 model levels (from the surface up to roughly 120 hPa) are employed. The analysis domain encompasses northern Africa and Europe, specifically from 30° W to 60° E and 15° to 73° N. For climatological reference, we use the 30-year period prior to the study period, hence January 1992 – December 2021. To cover the reference and study periods, 2m-temperature (t2m) data are acquired for January 1992 – April 2024.

3.2 Lighting data

A lightning measurement data set is used as a proxy for thunderstorm location. We use data from the lightning location network "Blitzortung" (Wanke et al., 2014). A large number of volunteers around the world have contributed to this network by setting up very low-frequency sensors. The network allows to reliably locate widespread lightning activity, although it cannot detect weak strokes at this frequency range. The detection efficiency varies slightly between day and night, but the location of widespread lightning activity can be detected reliably. Data are aggregated to the ERA5 grid and timestamps are floored to the previous full hour to match the hourly resolution. This results in a binary data set of flash-hours per ERA5 grid-cell. We omit data where only a single flash was observed within a radius of one ERA5 grid cell, to avoid erroneous outliers. In this work, "lightning occurrence" or "lightning probability" will refer to these binary, cell-aggregated lightning data, not individual strokes.

3.3 Atmospheric composition reanalysis

The fourth generation ECMWF global reanalysis of atmospheric composition, EAC4 (ECMWF Atmospheric Composition Reanalysis 4; Inness et al., 2019), is used as a dust reanalysis product. It provides dust aerosol optical depth at 550 nm (duaod550) at a 3-hourly resolution and 0.75° grid spacing. For comparability, we remap and interpolate the EAC4 data to match the spatio-temporal resolution of the ERA5 data. Dust aerosol optical depth (duaod550) is a single level variable which we use to determine unusually dusty periods during the study time period. Since the EAC4 data is only available from 2003 onwards, the years 2003-2021 are used for climatological reference in this case, and duaod550 data is acquired for the reference period and the study period, hence January 2003 – April 2024.

4 Methods

A trajectory model is needed for the AD detection (LAGRANTO, Sect. 4.1; Sprenger and Wernli, 2015). The detection of the AD edge, as well as the cap are explained in Sections 4.2 and 4.3. Some statistical considerations are presented in Section 4.4.

4.1 Trajectory calculation and detection of the atmospheric desert air mass

The calculation of the trajectories and detection of the AD air mass follows Fix-Hewitt et al. (2026). Trajectories are calculated forward in time with the Lagrangian Trajectory Analysis Tool (LAGRANTO; Sprenger and Wernli, 2015). They are initiated hourly along a 'curtain' marking the northern boundary of the source region in North Africa. The spatial resolution is 5 km in the horizontal and 10 hPa in the vertical between 1100 and 400 hPa. Only those trajectories are calculated forward that have a

https://doi.org/10.5194/egusphere-2026-2350
Preprint. Discussion started: 8 May 2026

northward (Europe-ward) wind component and start below the interpolated boundary layer height BLH_i (interpolated between daily maxima of the BLH, as a way to take into account former BLH air that is above the night-time BLH). Trajectories are integrated for 120 h. This results in approximately 108 million trajectories, of which 61 million pass 37° N and are therefore taken into account in this analysis. Trajectories are aggregated to grid boxes of 0.25°×0.25°×500 m. Any such grid box containing at least one trajectory is defined as an AD-cell. Often it is only of interest whether AD air is present anywhere above an ERA5-cell, hence if there is any AD-cell in the column, this is defined as an AD-column. Fore more details on the detection method refer to Fix-Hewitt et al. (2026).

4.2 Detection of the AD edge

In order to analyse effects (especially thunderstorm occurrence) that are connected to the edge of the AD, the air mass edge has to be detected from the binary AD-cell data in a respective layer, L. To achieve a smoother edge, small holes and speckle were removed before detecting the edge. This is done using mathematical morphology operations used in image processing (closing, opening, erosion). A more detailed description and schematic figure of the edge detection algorithm can be found in the appendix (Sect. A1). We applied the edge detection algorithm to individual levels (1500, 2000, 2500 m) and to 1.5 km thick layers (AD-cell centre in 1–2 km, 1.5–2.5 km, 2–4 km). It is found that the results are not very sensitive to the choice of altitude or layer thickness (Fig. A2, A3), but using a layer of 1.5 km (3 levels) instead of only one level makes the edge less noisy. Hence, we chose to detect the AD edge in a layer, approximately at and above the local BL, between 1250 and 2750 m (AD cell centres in 1.5, 2, and 2.5 km), which also includes the 800 hPa edge of the AD, where lightning occurred in the study by Fix et al. (2024).

To assess effects caused by proximity to the edge or the air mass centre, we classify grid cells by their distance to the AD edge. Let d be the shortest distance from a cell to the detected edge (Euclidean distance in number of cells), and $D_1 < D_2$ two distance criteria. Then all cells with $d < D_1$ are 'near-edge', and those with $d \geq D_2$ and within the region with AD present in the layer between 1250 and 2750 m ($L = \mathrm{True}$) are in the 'AD centre'. Cells with $D_1 \leq d < D_2$ and $L = \mathrm{True}$ are not classified as either 'near-edge' or 'centre' to allow for a clear separation between 'near-edge' and 'centre' cells. Cells with $d \geq D_2$ and $L = \mathrm{False}$ are not considered, as they are neither close to the edge nor within the AD centre, even if they might have AD air present at levels not considered in L. We conducted a sensitivity study for different distance thresholds and find that the results do not vary much whether $D_1 = 5$ or 10 cells (approx. 150 or 300 km, Fig. A2). We therefore adopt $D_1 = 5$ (≈150 km) cells for the near-edge definition. Increasing D_2 from 10 to 15 or 20 cells substantially reduces the number of AD-centre cells, hence the number of observations to interpret (Fig. A3). We use $D_2 = 10$ cells (≈300 km) for the AD centre definition, to retain as many observations as possible. We consider 10 cells sufficiently far from the edge to avoid edge-related influences.

4.3 Detection of the cap

Previous literature about EMLs suggests that these air masses form a cap on top of the local BL, which is characterised by a strongly stable temperature profile, which caps the local BL underneath and prevents it form growing, which can lead to heat buildup in the BL (e.g. Carlson and Ludlam, 1968; Cordeira et al., 2017). In order to investigate whether ADs also form

https://doi.org/10.5194/egusphere-2026-2350
Preprint. Discussion started: 8 May 2026

a similar cap and whether its occurrence is related to positive temperature anomaly events or thunderstorm suppression, we developed a detection algorithm for the 'cap'. An ERA5 cell is identified to have a cap, when the lowest trajectory in this column at that time is between the ERA5 BLH and BLH+500 m, and the stratification in that 500 m-layer is nearly isothermal, i.e. $\partial\theta/\partial z\,|_{\mathrm{aboveBLH}} \geq 10\,\mathrm{K\,km^{-1}}$. As in Fix-Hewitt et al. (2026), we only conduct this analysis during daytime hours (6 h, 10:00 through 15:00 UTC), to capture a period during which the ERA5 BLH reaches its maximum. The definition of the cap here differs from the definition of the lid in Fix-Hewitt et al. (2026), because we require a minimum potential temperature gradient in the 500 m-layer above the BLH.

4.4 Statistical considerations

We identify periods with positive temperature anomaly and dust events, receptively, using standardised anomalies of t2m or duaod550. Climatological reference periods are chosen as 1992–2021 for t2m and 2003–2021 for duaod550 (data availability from 2003 onward). Because a climate-change signal can be expected in t2m, the full t2m time-series (01/1992–04/2024) is detrended prior to anomaly calculation. For each hour of the year, we define the climatological background as the median over the respective reference period, denoted $\mathrm{median}_{\mathrm{clim}}(x)$, and the corresponding climatological standard deviation $\sigma_{\mathrm{clim}}(x)$. To smooth out synoptic scale variations, a 4th-order Butterworth low-pass filter is applied using a 30 d cutoff period. To preserve the diurnal cycle, the filtering is performed separately for each hour of the day for t2m. Standardised anomalies are then calculated as:

$$x' = \frac{x - \mathrm{lowpass}(\mathrm{median}_{\mathrm{clim}}(x), f_c = 1/30\,\mathrm{d}^{-1})}{\mathrm{lowpass}(\sigma_{\mathrm{clim}}(x), f_c = 1/30\,\mathrm{d}^{-1})} \tag{1}$$

where x is the respective variable (duaod550 or detrended t2m) and x' is its standardised anomaly. Strong and extreme events are defined by thresholds of 2, and 4, respectively (as in Gkikas et al., 2009). In the current work, results are shown for strong events (Event = $x' > 2$), results for extreme events (extreme Event = $x' > 4$) are presented and briefly discussed in the Appendix (See Sect. C). It should be noted that individual hours are treated as individual events in this study.

We assess whether the probability of an extreme weather event increases in the presence of an AD using conditional probabilities and odds ratios (OR; similar approaches used in Stephenson, 2000; Mohr et al., 2019; Röthlisberger and Martius, 2019; Taszarek et al., 2020). The conditional probability $P(\mathrm{Event} \mid \mathrm{AD})$ can be understood in two ways: What percentage of AD occurrences comes with an event? Or: How likely is an event to occur, given AD air is present?

Rather than comparing the conditional probabilities for occurrence vs. non-occurrence of an event directly – conditional on presence vs. absence of an AD – we consider standardised log-odds ratios $\ln \mathrm{OR}_{\mathrm{std}}$ (Stephenson, 2000). These are normalised statistics that factor in all four possible combinations of the conditional probabilities described above, while accounting for differences in the variability due to different marginal probabilities. Thus, the resulting $\ln \mathrm{OR}_{\mathrm{std}}$ are centred around zero with positive values indicating increased odds of the event in the presence of AD or decreased odds in the absence of ADs. Negative values indicate decreased odds in the presence of AD or increased odds in its absence. Larger magnitudes indicate stronger evidence relative to sampling variability. Increased odds can indicate that the event may be a consequence of an AD, or they have a common driver. This analysis is applied for positive temperature anomaly and dust events. For the 'Event' being

https://doi.org/10.5194/egusphere-2026-2350
Preprint. Discussion started: 8 May 2026

lightning the same analysis is additionally done with 'near AD edge' and 'in AD centre' as the conditioning probabilities. The log-odds ratio then compares the conditional probabilities under the conditions 'near AD edge' or 'AD centre' and 'neither within AD nor near its edge'. More details about the conditional probabilities, odds ratio and the equation for its standard error can be found in the Appendix (Sect. A2). Log-odds ratios and (Conditional) probabilities are shown for several variables, the quantities are the same, but the colour scales may vary to ensure visibility for different magnitudes.

5 Results and discussions

In the following section the results are presented and discussed for positive temperature anomalies (Sect. 5.1), thunderstorms (Sect. 5.2), and dust (Sect. 5.3). To make it easier to follow, the results (Sects. 5.1.1, 5.2.1. 5.3.1) are immediately followed by their discussion (Sects. 5.1.2, 5.2.2. 5.3.2). Combined summary and conclusions from these are given in Sect. 6.

5.1 ADs and positive temperature anomalies

In this section, the co-occurrence of positive temperature anomalies (PTAs) with ADs is investigated. Results are shown in Sect. 5.1.1 before they are discussed in Sect. 5.1.2.

5.1.1 Co-occurrence of positive temperature anomalies with ADs

The co-occurrence of positive temperature anomalies and AD is investigated using the conditional probability and the standardised $\ln \mathrm{OR}$ for a positive temperature anomaly event given the presence of AD air. An ERA5-cell experiences a positive temperature anomaly event, when the standardised 2m-temperature anomaly (t2m', Eq. 1) exceeds 2 at the given time. Figure 1a shows the total, unconditional probability of a positive temperature anomaly event $P(\mathrm{PTA\ Event})$. In some regions, particularly in western Europe and over the sea, positive temperature anomaly events occur in more than 9% of the time during the study period. Figure 1b shows the probability of a positive temperature anomaly event, given the presence of an AD ($P(\mathrm{PTA\ Event} \mid \mathrm{AD})$, shading), and the conditioning probability $P(\mathrm{AD})$ (contours). Conditional probabilities are highest in an arc from southwestern to northern Europe, where temperatures are unusually high during more than 10% of the time that AD air is present. Figure 1c shows the standardised $\ln \mathrm{OR}$, which compares the odds of a positive temperature anomaly event during AD periods and AD-free periods. Positive values (green colours) in Fig. 1c indicate that positive temperature anomaly events are more likely to occur in the presence of AD than during its absence. It is obvious that this is the case in most of the domain, and the large values indicate strong evidence with respect to the variability. The strongest effect is visible over the bay of Biscay and the British Isles, as well as over the Mediterranean Sea and regions neighbouring the Baltic Sea, while in the Alps and over the Anatolian peninsula the effect is much smaller or non-existent. This pattern is also reflected in the mean and median of t2m' during AD and non-AD periods: The mean and median are elevated during AD periods compared to non-AD periods in the entire domain (median is shown in Fig. B1 in the Appendix). This is strongest in the region of the Bay of Biscay and over the British Isles, where AD periods have up to 1 K higher standardised anomalies on average.

https://doi.org/10.5194/egusphere-2026-2350
Preprint. Discussion started: 8 May 2026

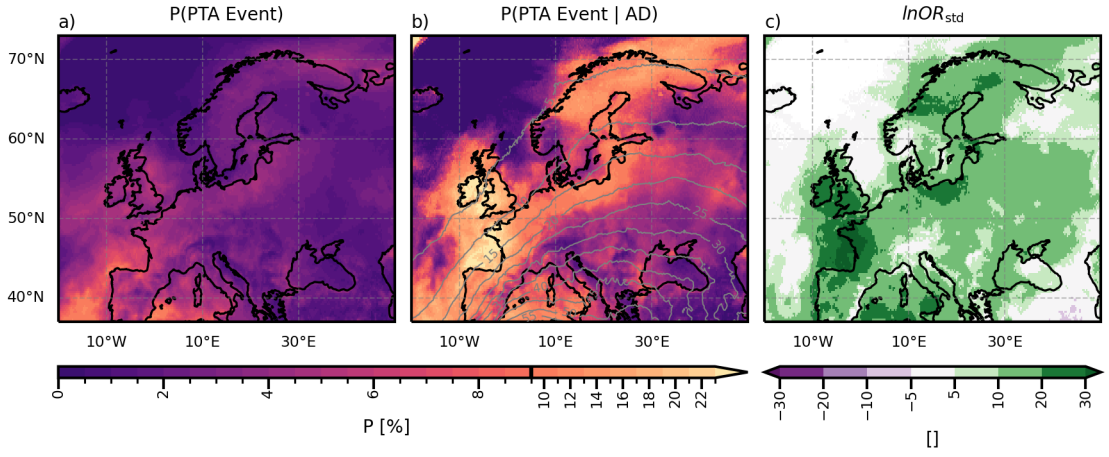

Figure 1. (a) Total probability of a positive temperature anomaly event (PTA event, t2m'>2) per grid cell and hour. **(b)** Probability of a PTA event, given the presence of AD air. Contour lines show the conditioning probability, $P(\mathrm{AD})$, per cell and hour in percent, 5 percentage-points spacing. **(c)** Standardised $\ln \mathrm{OR}$ for a PTA event given AD presence. Note that the colourbar for the probabilities has irregular spacing to highlight gradients at both the low and high ends of the probability range.

The suggested mechanism for enhanced near-surface temperatures during an EML (and therefore during an AD) is trapping of heat below a layer of stable stratification (Cordeira et al., 2017). To investigate whether this is the dominant process here, instead of conditioning the positive temperature anomaly on the presence of the AD, we now condition it on the presence of an AD with a cap (Sect. 4.3). It should be mentioned first that the cap is rare: the probability $P(\mathrm{Cap} \mid \mathrm{AD})$ is below 20% in the entire domain, and exceeds 5% almost only above the sea (Fig. B2a). Its average duration is between 1 and 2 days across the domain (Fig. B2b) and 90th percentile durations exceed 3 days only in the Mediterranean (Fig. B2c). Figure 2a shows the conditional probability $P(\mathrm{PTA\ Event} \mid \mathrm{AD})$ again (as Fig. 1b, different colour scale for better comparability), while Figure 2b shows the probability of an PTA event conditioned on the presence of a cap, $P(\mathrm{PTA\ Event} \mid \mathrm{Cap})$. Figure 2b shows elevated values in the Mediterranean as well as off the western European coasts. The standardised $\ln \mathrm{OR}$ (Fig. 2c) shows that in most of the domain there is no significant effect (light colours), except in the eastern Mediterranean, where it is strongly positive (green) indicating that there positive temperature anomaly events are significantly more frequent in the presence of a cap compared to AD without cap. A smaller positive effect can be seen over the Black Sea.

5.1.2 Discussion of positive temperature anomalies

A striking feature in Fig. 1a is the elevated probability of positive temperature anomalies in the western Mediterranean Sea and the Atlantic, especially close to the Iberian and French coasts. A likely explanation are marine heatwaves in the North Atlantic as well as the Mediterranean during the study period (e.g. Juza et al., 2024; England et al., 2025). Leaving the respective periods (summer 2022 and summer 2023) out does indeed reduce probability of positive temperature anomaly events in the

https://doi.org/10.5194/egusphere-2026-2350
Preprint. Discussion started: 8 May 2026

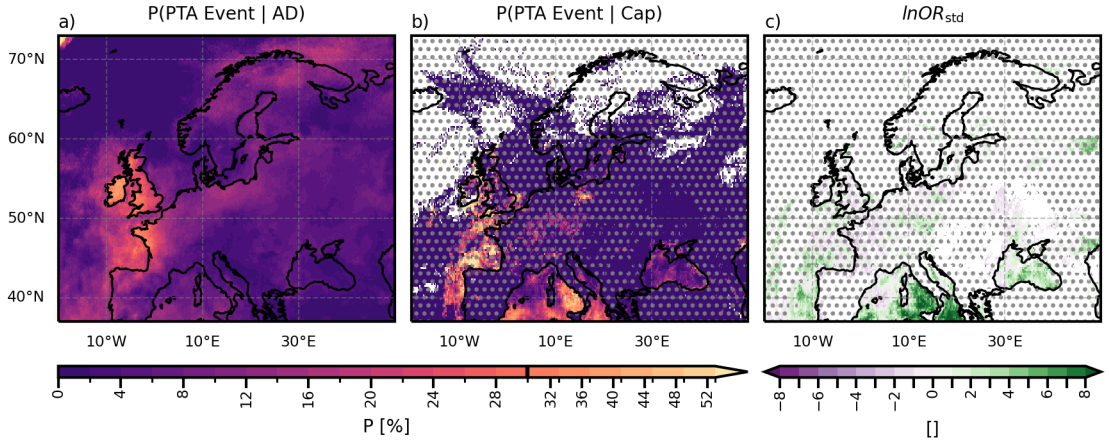

Figure 2. (a) Probability of a positive temperature anomaly event (PTA event, t2m'>2) given the presence of AD air (as panel b in Fig. 1, different colour scale for better comparability) per grid cell and hour. **(b)** Probability of a PTA event, given the presence of AD with a cap. **(c)** Standardised $\ln \mathrm{OR}$ for a PTA event given cap presence. Note that the colourbar for the probabilities has irregular spacing to highlight gradients at both the low and high ends of the probability range. Stippling indicates where only 1% or less of the time series ever experience an AD with a cap ($P(\mathrm{AD} \cap \mathrm{Cap}) \leq 1\%$).

North Atlantic around the British Isles and in the western Mediterranean. However, leaving these periods out for the entire analysis will reduce the 2-year dataset drastically, which is especially problematic as that leaves no data for summer. Using longer time series to reduce the influence of these periods is not feasible due to data storage constraints.

The standardised $\ln \mathrm{OR}$ is largest in the Bay of Biscay and over the British Isles, as well as over the western Mediterranean Sea, indicating that the effect of the presence of AD air on positive temperature anomalies is strongest there. Interestingly, the British Isles experience AD air less than 10 % of the time, but more than 20 % of those cases co-occur with positive temperature anomalies. Several studies observe warm temperature anomalies over the UK during Spanish Plume events (de Villiers, 2020; Sibley, 2012). The Spanish Plume is an EML originating over the Iberian Peninsula, although the term has frequently been misused (Schultz et al., 2025b). Some studies suggest that during Spanish Plume events air also originates in northern Africa (Sibley, 2012; de Villiers, 2020; Schultz et al., 2025a), so that some Spanish Plume air streams can be seen as a subset of or related to ADs.

Elevated terrain. In Figure 1c the Alps and the Anatolian peninsula stand out as the only land regions that do not have a strongly positive standardised log-odds ratio. In these regions, also the probability of intrusion of AD air into the local BL is elevated (Fix-Hewitt et al., 2026, their Fig. 7). This indicates that while the BL in these regions may frequently reach potential temperatures similar to those in the AD, making penetration possible, other processes are more dominant in producing strong positive temperature *anomalies*. This is not the case for all regions with elevated terrain, however, the most prominent counterexample being the Iberian peninsula. There, the terrain is also elevated, so is the probability for AD air intruding the local BL, but still the probability of positive temperature anomaly events is clearly elevated in the presence of AD air (Fig. 1b,c).

https://doi.org/10.5194/egusphere-2026-2350
Preprint. Discussion started: 8 May 2026

Capping inversion. Fix-Hewitt et al. (2026) already showed that it is not so common that the AD resides close to the local BLH and forms a lid, and that when it does, the duration is only few days (Fix-Hewitt et al., 2026, their Fig. 6). Additionally requiring the layer above the local BL to be roughly isothermal, results in caps that are even rarer and shorter (Fig. B2), which reduces their ability to cause heat-buildup underneath over time. It was shown in Sect. 5.1.1 that the probability of positive temperature anomaly events is significantly increased in the presence of AD air, however, only in the Mediterranean and over the Black Sea it could be tied to the presence of the cap (Fig. 2c, daytime hours only). This is likely due to different BL properties over the sea. Marine BL are typically cooler and moister during daytime (e.g. Garratt, 1994), so that AD air will remain well separated and caps are hence more frequent. Also, the proximity to the source region plays a role: First, the AD altitude is typically lower (Fix-Hewitt et al., 2026), making it more probable that AD air resides right above the local BL. Second, the less time the AD air had to travel, the less it could be modified, making it likely that it is still very warm and stably stratified.

Preferential warming on the upstream side of ridge axis. In Fix-Hewitt et al. (2026) 66 extensive AD events were identified. 19 of those have a positive temperature anomaly event in at least 10% of the area covered by the AD (north of 37°N). Often, the area with positive temperature anomaly events is on the upstream side of the ridge axis, sometimes coinciding with areas without or with only high clouds (not shown). We do not have further explanation for this behaviour and further investigations are beyond the scope of this study or the available data (i.e. ERA5 is not informed of the aerosol optical depth, hence its radiation variables are of limited use).

Positive temperature anomalies frequently co-occur with ADs, but this does not necessarily imply a causal relationship. It was mentioned by Carlson and Ludlam (1968) that already one day of insolation in the presence of a capping EML can be enough to increase the (wet-bulb) temperature in the underlying BL significantly and Fix-Hewitt et al. (2026) showed that the average duration of AD streaks are below one day for most of the domain (their Fig. 4). We therefore think that investigating the direct co-occurrence of positive temperature anomaly events and AD presence is insightful, however, we cannot exclude that there are time-lagged effects that are not captured in our analysis. While AD-related caps may favour heating in some regions, high near-surface temperatures during ADs can also arise from diabatic heating, subsidence-driven adiabatic warming, and/or warm-air advection (Röthlisberger and Papritz, 2023). Disentangling these contributions and whether or how they are related to ADs or confounding factors is beyond the scope of this study.

However, some processes that have been described in the context of heat waves do have similarities with ADs: Cos et al. (2025) describe low-level warm air intrusions from the Sahara into the Mediterranean, although Zschenderlein et al. (2019) find horizontal advection to play a minor role in European high temperatures. When air ascends in a warm conveyor belt, it releases latent heat and brings low potential vorticity air to higher levels, which can lead to an intensification of the ridge (or even atmospheric blocking; Pfahl et al., 2015). Since one air stream identified within the AD is similar to a warm conveyor belt (although from a drier source region), and ADs often occur together with amplified ridges (Fix-Hewitt et al., 2026), ADs may also intensify these ridges. High temperatures can be observed in ridge situations, and especially in summer they are caused by diabatic heating due to increased insolation, and to a lesser degree due to adiabatic heating from subsidence (Sousa et al., 2018).

https://doi.org/10.5194/egusphere-2026-2350
Preprint. Discussion started: 8 May 2026

5.2 ADs and thunderstorms

EMLs are known to suppress thunderstorms in their centre due to a cap, while they tend to erupt violently along their edges (e.g. Carlson and Ludlam, 1968; Keyser and Carlson, 1984; Farrell and Carlson, 1989; Cordeira et al., 2017; Ribeiro and Bosart, 2018, and many more). In the following, we examine whether this also holds for the more general case of ADs.

5.2.1 Occurrence of lightning along the AD-edge versus in the AD-centre

Lightning throughout the year is a rare event locally. The unconditional probability of lightning is generally below 2% (Fig. 3a). Higher probabilities coincide with land areas, especially mountainous regions (see white contours, Fig. 3a), where orographic lifting of the larger scale flow and orographically induced circulations provide additional mechanisms for releasing CAPE (in agreement with Enno et al., 2020). Figure 3b shows that lightning probability approximately doubles when AD air is present in the levels 1.5, 2, and 2.5 km. Over the Mediterranean, this is the case in up to 40% (grey contours, Fig. 3b). Also the standardised log-odds ratio confirms that lightning is more likely in the presence of AD air at those levels than its absence by being strongly positive (green, Fig. 3c) in large parts of the study region.

ERA5 grid cells can be within a swath of about 1.25° (5 cells) on either side of the AD edge in an astonishing 30% of the time in the Mediterranean (Fig. 3d, grey contours). This probability gradually decreases northwards to 5% in northern Europe. In a large part of the domain, the probability of lightning is strongly elevated, given an AD edge is close (Fig. 3d, shading), which is also supported by strongly positive values in the standardised log-odds ratio (green, Fig. 3e). In fact, almost 27% of all lightning occurs within the 5 cell margin around the AD edge (not shown).

The probability of an ERA5 cell being in the centre of an AD (at least 5 cells $\approx 2.5°$ interior of the edge) is lower with 10% in the Mediterranean, decreasing northwards and being negligible in northern Europe (Fig. 3f, grey contours). Surprisingly, also the probability of lightning given the presence of the AD centre is elevated (Fig. 3f, shading). The standardised log-odds ratio (Fig. 3g) highlights again that lighting is more frequent also in the centre of an AD, albeit over a smaller part of the domain than it is the case for the AD edge (Fig. 3e).

5.2.2 Discussion of lightning occurrence

It is surprising that the lightning probability is increased in the presence of the AD (Fig. 3f,g), as it could be expected that thunderstorm eruption is hindered by a capping inversion that forms in the AD centre. However, as already mentioned in Section 5.1, the occurrence of a cap is rare, and the probability of it occurring in the AD centre, $P(\mathrm{Centre} \cap \mathrm{Cap})$, is negligible (exceeds 1% only over the Mediterranean Sea). While strong convective inhibition (CIN) hinders convection, medium values of CIN (50-200 $\mathrm{J\,kg^{-1}}$) can actually be favourable, as they allow build-up of CAPE before strong enough triggers overcome the inhibition (Andrews et al., 2024).

Conditionally unstable stratification in AD centre regions. Air that originates within a deep, warm CBL in the source region is typically well mixed with a near–dry-adiabatic lapse rate. If this air is advected downstream with modest modification it causes steep lapse rates and conditionally unstable stratification over a moister local BL. Once CIN is overcome, e.g. by

https://doi.org/10.5194/egusphere-2026-2350
Preprint. Discussion started: 8 May 2026

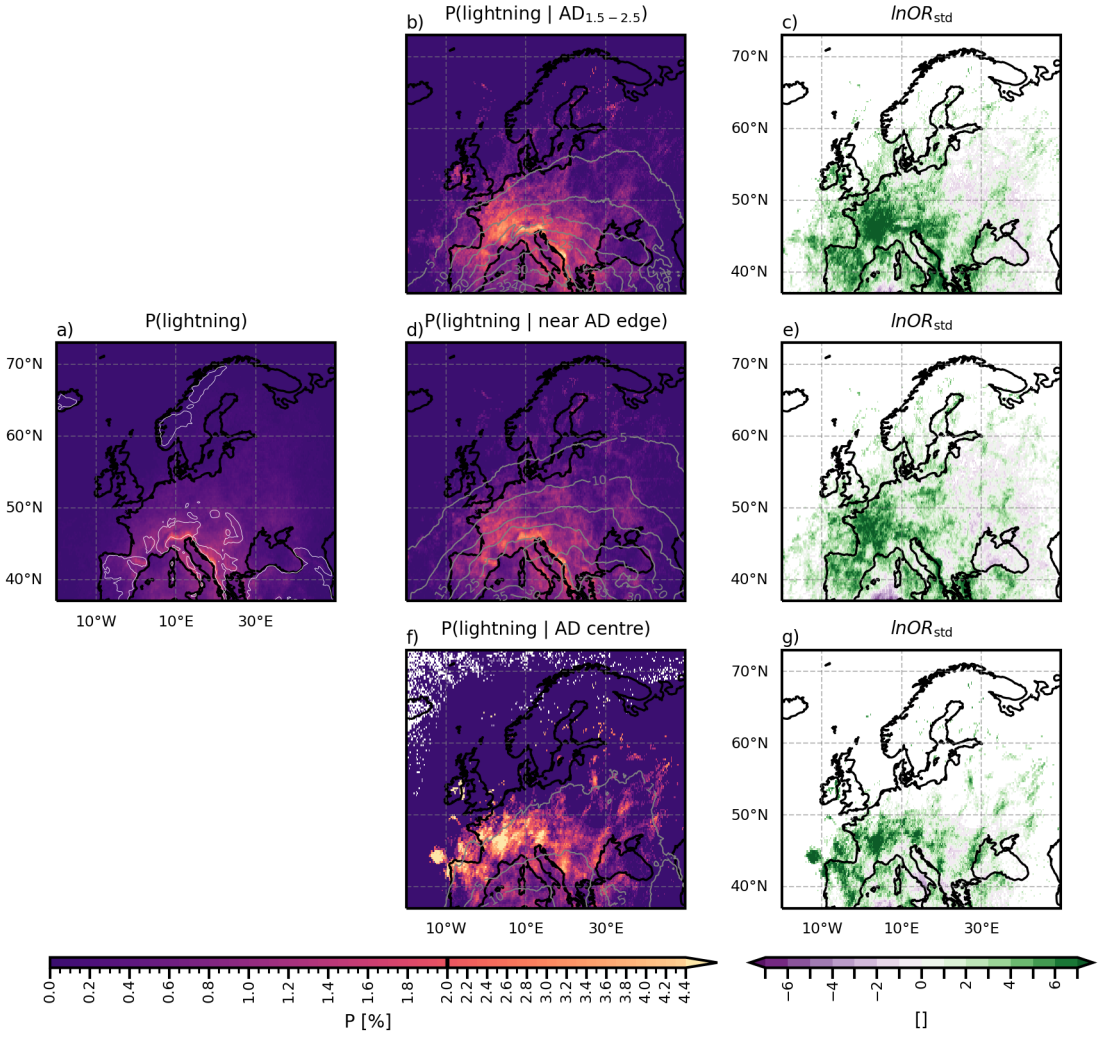

Figure 3. **(a)** Total probability of lightning per grid cell and hour. White contour lines indicate the 600 m topographic isoline. **b)** Probability of lightning, given AD air is present at the 1.5, 2, and 2.5 km levels ($AD_{1.5-2.5}$). Contour lines show the conditioning probability, $P(AD_{1.5-2.5})$, per cell and hour in percent, 5 percentage-points spacing. **(c)** Standardised ln OR of lightning within $AD_{1.5-2.5}$. **(d)** Probability of lightning, given it is close to the AD edge. Contour lines show the conditioning probability, $P(\text{near AD edge})$, per cell and hour in percent, 5 percentage-points spacing. **(e)** Standardised ln OR of lightning near AD edge. **(f)** Probability of lightning, given it is within the AD centre (≥10 cells away from edge). Contour lines show the conditioning probability, $P(\text{AD centre})$, per cell and hour in percent (contours for 1, 5, and 10% are shown). **(g)** Standardised ln OR of lightning in the AD centre. Note that the colourbar for the probabilities has irregular spacing to highlight gradients at both the low and high ends of the probability range.

https://doi.org/10.5194/egusphere-2026-2350
Preprint. Discussion started: 8 May 2026

surface heating, low-level convergence, or synoptic ascent, deep moist convection can initiate even in the centre of the AD. Due to horizontal heterogeneities in the source region, also the cap can be heterogeneous, which can allow for localised outbreaks in spots with lower CIN within regions with a cap (Farrell and Carlson, 1989).

To test this hypothesis, we look at CIN and the presence of conditionally unstable stratification in the 2 km above the local BLH during daytime hours (Fig. 4). A layer is conditionally unstable when the potential temperature gradient $\partial\theta/\partial z = (\theta_{\mathrm{BLH+2km}} - \theta_{\mathrm{BLH}})/2\,\mathrm{km}$ is less than $3.5\,\mathrm{K\,km^{-1}}$. The top row of Fig. 4 (a-d) shows conditions along the edge of the AD, the bottom row (e-h) in its centre. On average, the layer above the BL is conditionally stable everywhere along the AD edge (grey colours in Fig. 4b). Also in the AD centre the layer is predominantly conditionally stable (grey colours in Fig. 4f) with the exception of the Iberian Peninsula, parts of France and parts of southern Europe. In situations with lightning, however, this changes dramatically with most parts being conditionally unstable in the course of the day (yellow-orange colours in Fig. 4c and g) – both along the AD edge and in the AD centre. On such days, CIN is also in a favourable range of less than 200 J/kg (Fig. 4d and h). These results thus support the hypothesis that a conditionally unstable layer provided by the AD with modest CIN values underneath makes it possible for thunderstorms to occur even in the centre of an AD. This therefore provides an explanation for why the standardised log-odds ratio for lightning both near the AD edges and in the AD centre indicates that the situation is supportive of thunderstorm occurrence (Fig. 4a,e, green colours). These results can be expected also approximately hold when taken over the whole day instead of daytime only. While this is a new result, the finding that the combination of conditionally unstable AD air and modest CIN leads to thunderstorms along the edges of ADs has been extensively documented (for the special case of EMLs, e.g. Carlson and Ludlam, 1968; Carlson et al., 1983; Keyser and Carlson, 1984; Farrell and Carlson, 1989; Lanicci and Warner, 1991b; Johns and Dorr, 1996; Banacos and Ekster, 2010; Lewis and Gray, 2010; Dahl and Fischer, 2016; Ribeiro and Bosart, 2018; Li et al., 2021).

Baroclinic zone and ageostrophic circulation at AD edges. Several past studies have investigated the eruption of particularly violent thunderstorms near the edges of EMLs. It is described that near the edge, a convergence zone forms, possibly ahead of a cold front or dryline (Carlson et al., 1983; Keyser and Carlson, 1984; Dahl and Fischer, 2016). In this region a strong stability gradient is present (Carlson et al., 1983) and it is characterised by a baroclinic zone. Keyser and Carlson (1984) describe describe how due to confluence and anticyclonic shear in this baroclinic zone, a thermally direct ageostrophic circulation forms at the midlevel air mass boundary, while a thermally indirect cell forms higher up. This leads to ascent near the EML edge, which is likely too weak to initiate convection, but can diminish the strength of the cap and, together with other lifting mechanisms, lead to the initiation of thunderstorms along EML edges. Another mechanism fostering convective outbreaks near EML edges is 'underrunning' (Carlson et al., 1983; Farrell and Carlson, 1989), where the moist and heated air in the local BL moves horizontally, until it reaches the lateral edges of the EML, where inhibition is weaker, so that convection can occur.

These general results are also supported by Feldmann et al. (2025) who find that western and central Europe are regions with "temperature-limited severe convective outbreak types". In temperature-limited regions, the advection of warm and moist air leads to instability. Convective outbreaks happen on the western flank of a ridge, ahead of a trough, and strong positive temperature anomalies are found within the ridge – hence, a synoptic set-up that is similar to those leading to ADs, and convective outbreaks in regions where their edges can be expected. They also appreciate the role of EMLs for these types. In

https://doi.org/10.5194/egusphere-2026-2350
Preprint. Discussion started: 8 May 2026

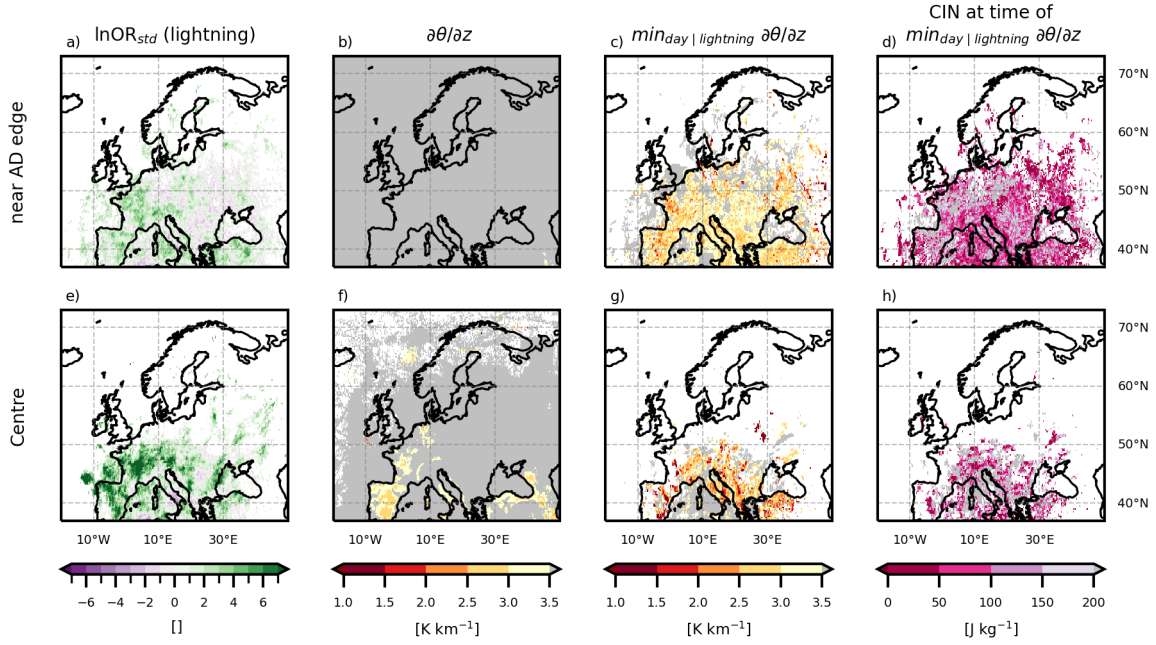

Figure 4. Daytime hours (10-15 UTC) only. Panels **(a)-(d)** show results for near AD edge cells, panels **(e)-(h)** for AD centre cells. Panels **(a), (e)** show the standardised ln OR for lightning occurrence, given the proximity of the AD edge **(a)** or the presence of the AD centre **(e)** (as Fig. 3e,f, but for daytime only). Panels **(b), (f)** show the average $\partial\theta/\partial z$ in the 2 km above the local BLH, given the cell is near the AD edge **(b)** or in its centre **(f)**. Panels **(c)** and **(g)** show average daily minimum $\partial\theta/\partial z$, where the daily minimum is computed from only those sub-daily samples when the cell is classified as near-edge **(c)** or centre **(g)**. The average is built only over those days that have a lightning occurrence near the AD edge **(c)** or in its centre **(g)** at least once that day. Panels **(d)** and **(h)** show the average CIN for those same time steps.

parts of eastern Europe, the Slavic and Balkan regions the standardised log-odds ratio of lightning occurrence near the edge is small, or even negative. This implies that in these regions the presence of the AD edge does not foster thunderstorm formation. Feldmann et al. (2025) find that thunderstorm formation in these regions is saturation-limited, which means a positive relative humidity anomaly is important for the formation of thunderstorms. This can explain why thunderstorms may not form even in favourable environments near the AD edges, if the necessary humidity anomaly is not present.

5.3 ADs and dust

Dust can be swept up into the CBL in the arid and desert source regions of ADs and subsequency lead to dust events in the target regions. In Sect. 5.3.1 we show how often ADs co-occur with dust events, which is then discussed in Sect. 5.3.2.

https://doi.org/10.5194/egusphere-2026-2350
Preprint. Discussion started: 8 May 2026

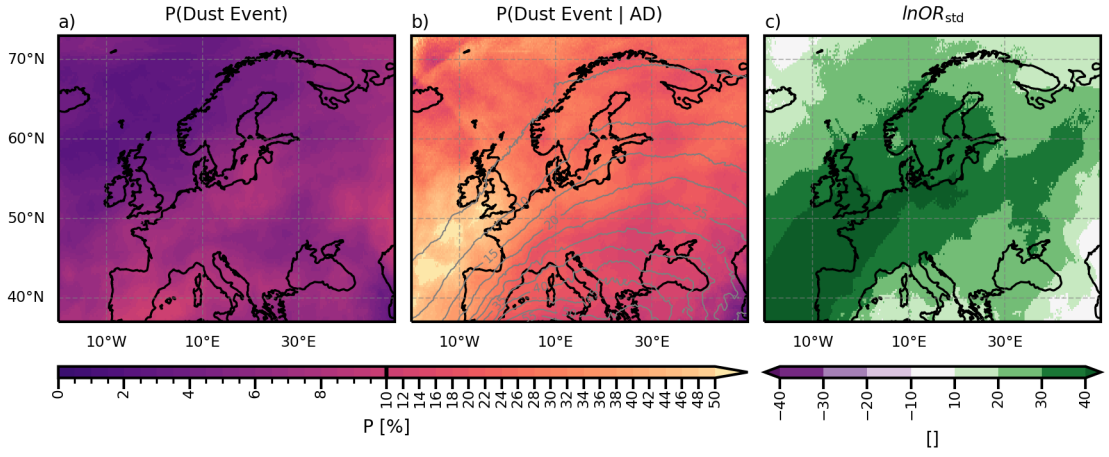

Figure 5. (a) Total probability of a dust event (duaod'>2) per grid cell and hour. **(b)** Probability of a dust event, given the presence of AD air. Contour lines show the conditioning probability, $P(\mathrm{AD})$, per cell and hour in percent, 5 percentage-points spacing. **(c)** Standardised $\ln \mathrm{OR}$ for a dust event given AD presence. Note that the colourbar for the probabilities has irregular spacing to highlight gradients at both the low and high ends of the probability range.

5.3.1 Co-occurrence of dust and ADs

We classify a dust event, when the standardised dust aerosol optical depth at 550 nm anomaly (duaod550', Eq. 1) exceeds 2 at the given time. Figure 5a shows the total, unconditional probability of dust events, $P(\mathrm{dust})$. The Mediterranean region experiences strong dust events more than 9% of the time, and also regions around the Baltic Sea and north-east of the Black Sea have elevated dust event probabilities. It becomes apparent that the pattern of the unconditional probability for dust (Fig. 5a, shading) is similar to the pattern of the probability of AD (Fig. 5b, contours), with higher values in the southern part of the domain, and a north-eastward extension of the region with elevated values. Figure 5b shows the probability of a dust event, given the presence of an AD ($P(\mathrm{Dust\ Event} \mid \mathrm{AD})$, shading), and the conditioning probability $P(\mathrm{AD})$ (contours, same as in Fig. 1b). Conditional probabilities are elevated compared to the unconditional probability throughout the domain, and they are highest north and northwest of the Iberian peninsula - in regions, where ADs occur in less than 10% of the time. Figure 5c shows the standardised $\ln \mathrm{OR}$, which compares the odds of a dust event during AD periods and AD-free periods. Positive values (green colours) in Fig. 5c highlight that dust events are more likely to occur in the presence of AD than during its absence. It is obvious that this is the case everywhere in the domain, and the very large values indicate strong evidence with respect to the variability. This is most pronounced from the Iberian Peninsula, across the English Channel and to southern Scandinavia, but less pronounced over the Mediterranean and the far east of the domain. However even in the Mediterranean $\log \mathrm{OR}_{\mathrm{std}}$ exceeds 10, which is clearly robust with respect to the sample variability.

The conditional probability of dust events given that an AD is present in the column ($P(\mathrm{Dust\ Event} \mid \mathrm{AD})$; Fig. 5b, shading) also gives insight into what fraction of AD events are dusty. While the probability of AD ($P(\mathrm{AD})$; Fig. 5b, contours) decreases

https://doi.org/10.5194/egusphere-2026-2350
Preprint. Discussion started: 8 May 2026

towards the north and northwest, the probability of a dust event given the presence of AD ($P(\text{Dust Event} \mid \text{AD})$, Fig. 5b, shading) increases towards the northwest. Especially in the western part of the domain (western Europe and southern British Isles), more than 40 % of AD occurrences also bring dust events (yellow colours in Fig. 5b).

5.3.2 Discussion of dusty ADs

The pattern of $P(\text{Dust Event})$ (Fig. 5a) is similar to $P(\text{AD})$, and logically so. The probability for a dust event is highest closest to the source region, while regions further away have a reduced probability - because the dust-carrying air does not reach as far as often, and because more dust can be deposited during the longer journey. The only region that draws attention is the very east of the domain. Here, the probability of a dust event is higher than in neighbouring regions, and the effect of the AD is less pronounced (light colours in Fig. 5c). Additionally, east of 30°E is the only region, where $P(\text{dust event} \mid \overline{\text{AD}})$ exceeds 5%. This indicates that in the very east of the domain, the presence of ADs is not as important for the occurrence of a dust event as in the rest of the domain. Two reasons are possible: (1) The dust may originate from another AD source than used in our study such as the Arabian peninsula or central Asian arid regions. (2) The air may take longer than 120 h to reach eastern Europe and thus is no longer tracked as AD air by our algorithm.

These results are in agreement with the results from Hermes et al. (2024) (and Barkan et al., 2005) who find that dust over Europe typically occurs when a far-south-reaching trough over the Iberian peninsula, transporting dust towards Europe across the western Mediterranean. Cuevas-Agulló et al. (2024) find that during more than half of the late winter/early spring dust events in the western Mediterranean region, a cut-off low was present west of the Iberian peninsula. They also find increased blocking over the Euro-Atlantic sector. Israelevich et al. (2012) identify dust transport pathways towards Europe across the Mediterranean and via recirculation from the Atlantic. These are all synoptic situations and trajectory pathways that resemble those typical for ADs, found by Fix-Hewitt et al. (2026).

An interesting intersection with aerosol atmospheric rivers (AAR) and atmospheric rivers (ARs) emerges. ARs are narrow, elongated regions of elevated water vapour transport (Ralph et al., 2018). Chakraborty et al. (2021) apply this concept to narrow, elongated regions of aerosol transport and define AARs. They attribute 40-100% of the total aerosol transport to these AARs. By definition, AARs originating in the boundary layers of desert regions will also be ADs. A combination of the concepts is presented by Dezfuli et al. (2021) and Francis et al. (2022), who describe that ARs can pick up dust, when travelling over desert areas, forming dusty atmospheric rivers. The latter report that 78% of ARs crossing northwest Africa are linked to dust events in Europe. They also describe how the phenomena are interlinked: ARs cause higher near-surface wind, which makes dust air-borne. The radiative properties of the dust particles can then lead to a warming of the dust-laden layer, which can lead to more moisture uptake. In this context, it could be interesting for future research to examine the extent and nature of the overlap among (dusty) atmospheric rivers, aerosol atmospheric rivers, and atmospheric deserts.

https://doi.org/10.5194/egusphere-2026-2350
Preprint. Discussion started: 8 May 2026

6 Summary and conclusions

Atmospheric deserts (ADs) are air masses that are advected away from the convective boundary layers (CBLs) of their arid/desert source regions towards typically cooler/moister target regions. They are a generalisation of elevated mixed layers (EMLs), which are former boundary layer (BL) air masses that retain their well-mixed properties when advected over cooler, moister air masses, and often form a lid or capping inversion. Since ADs have been found to be frequent over Europe (Fix-Hewitt et al., 2026) and EMLs are known to influence thunderstorm and heat wave formation (e.g. Carlson and Ludlam, 1968; Carlson et al., 1980, 1983; Banacos and Ekster, 2010; Cordeira et al., 2017; Ribeiro and Bosart, 2018; Andrews et al., 2024), this study aimed to investigate whether ADs behave similarly. Due to their origin in North Africa, European ADs are also prone to bring dust towards Europe. In this study, we therefore addressed the co-occurrence of positive temperature anomalies, lightning, and dust events with ADs. Through investigation of conditional probabilities and standardised log-odds ratios, we come to the following conclusions:

1. The probability of anomalously high near-surface temperatures is significantly increased in the presence of ADs. However, the trapping of heat under a cap (e.g. Cordeira et al., 2017) did not emerge as the main driver.
2. Lightning occurrence is clearly enhanced near the AD edges in western and central Europe.
3. Lightning occurrence is also enhanced in the centre of ADs, favoured by conditionally unstable stratification AD air and modest CIN values.
4. Depending on the region, 10% to more than 40 % of the times AD air is present in Europe, it also carries anomalously high amounts of dust, and almost all dust events co-occur with ADs.

These findings lead to several topics that should be addressed in future research. Of particular interest are the causal relations. Why are ADs often accompanied by anomalously high near surface temperatures? Do they have a common driver, or could the AD be cause? Which processes lead to the triggering of thunderstorms near the AD edges? Can the suggested processes of underrunning (Farrell and Carlson, 1989) and ageostrophic circulations at a resulting convergence line (Dahl and Fischer, 2016) or mid-level baroclinic zone (Keyser and Carlson, 1984) be confirmed for ADs? What is the vertical distribution of dust within the AD and what influences does it have on e.g. temperature and cloudiness? While there are many open questions to be addressed, the findings in this study present a valuable next step towards establishing ADs as a new air stream type and valuable concept for understanding midlatitude weather.

Code availability. Much of the data processing is done with the climate data operators (`cdo`; Schulzweida, 2023) and `python`. All code used for the analysis is made available at https://doi.org/10.5281/zenodo.19658813 (Fix-Hewitt, 2026)

https://doi.org/10.5194/egusphere-2026-2350
Preprint. Discussion started: 8 May 2026

Data availability. ERA5 data is freely available at the Copernicus Climate Change Service (C3S) Climate Data Store (Hersbach et al., 2023). EAC4 data is freely available at the Copernicus Atmosphere Monitoring Service (CAMS) Atmosphere Data Store (Copernicus Atmosphere Monitoring Service, 2021). The results contain modified Copernicus Climate Change Service information 2020. Results are generated using Copernicus Atmosphere Monitoring Service information 2025. Neither the European Commission nor ECMWF is responsible for any use that may be made of the Copernicus information or data it contains. Lightning data from Blitzortung.org is available as participant of measurement network. LAGRANTO is available from: Sprenger and Wernli (2015).

Author contributions. GM and AZ acquired the funding for this project. All co-authors contributed to the study design. FFH conducted the calculations, the analysis, and wrote the manuscript under supervision by GM and AZ, with the support of IS and RS. IS and FFH acquired the data and RS supported in software development. GM, AZ, IS, and RS reviewed and revised the manuscript prepared by FFH.

Competing interests. The authors declare that they have no conflict of interest.

Acknowledgements. We thank Deborah Morgenstern for setting up LAGRANTO and running the first explorative trajectory calculations. We thank all colleagues who were involved in discussions, in particular also those the first author talked to at the Workshop on "Dynamics of Rossby Waves, Compound Extremes and Their Impacts" in Amsterdam (January 2026). The computational results presented have been achieved [in part] using the Austrian Scientific Cluster (ASC). This research was funded in whole by the Austrian Science Fund (FWF) 10.55776/P35780. For open access purposes, the authors have applied a CC BY public copyright license to any author accepted manuscript version arising from this submission. Large language models have been used to support code development and language improvements.

Appendix A: Detailed explanation of some methods

A1 Edge detection

The air mass edge is detected from the binary AD-cell data in a respective layer, L. This is done using mathematical morphology operations used in image processing. A layer L can consist of several levels, l. Hence, first, we combine the binary data of the altitude levels l by logical 'or' (Eq. A1, Fig. A1a-d). To avoid artificial edges at the domain edge, we pad L with replicate values (Fig. A1d, light grey). To fill small holes and reduce speckle, we apply multidimensional binary closing (Fig. A1e) followed by binary opening (Fig. A1f) with a structuring element S that includes all spatially neighbouring cells (including the diagonals, 3×3 Moore neighbourhood; Haralick et al., 1987), resulting in a smoothed binary dataset L_s. Then, edge cells are detected as the difference between the smoothed binary AD-cell data, L_s, and its erosion ($\ominus$, Eq. A2; Haralick et al., 1987, Fig. A1g, orange). All cells that are closer than D_1 cells to this edge, are defined as 'near edge' (here $D_1 = 5$, light orange in Fig. A1g). All cells that are at least D_2 cells from the edge but within L_s are considered as 'within the AD centre' (here

https://doi.org/10.5194/egusphere-2026-2350
Preprint. Discussion started: 8 May 2026

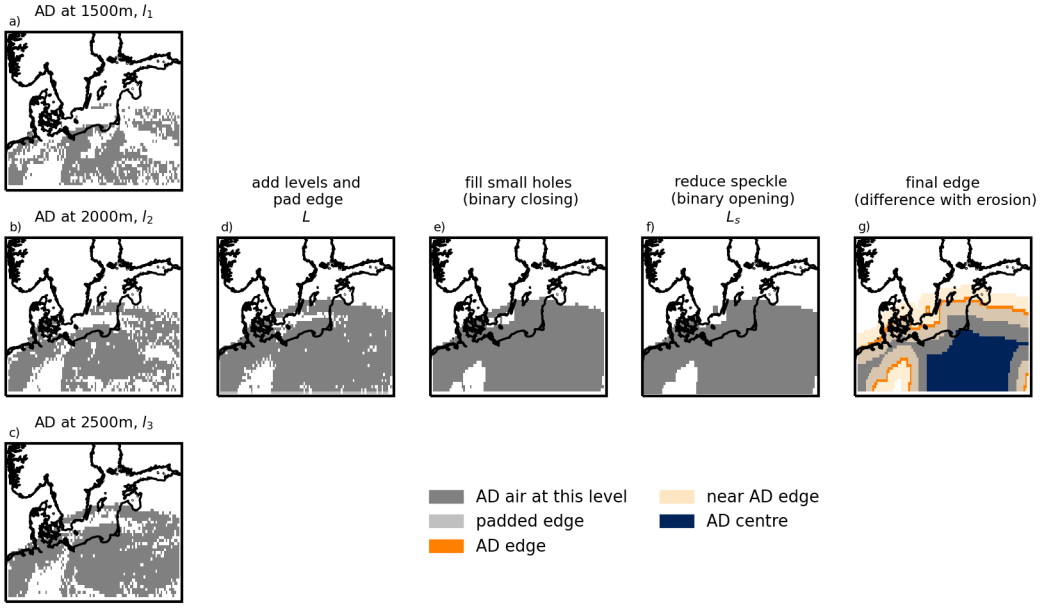

Figure A1. Schematic of edge detection algorithm. **9a-c)** AD extent at the respective levels 1500, 2000,and 2500 m. **d)** AD extent in the combined layer, L, according to Eq. A1. **e)** Small holes were filled, using binary closing. **f)** Speckle was removed using binary opening, results in smoothed AD extent L_s. **g)** Final result with smoothed AD extent (grey), AD edge (orange), cells near the AD edge (light orange), and cells within AD centre (dark blue).

$D_2 = 10$, dark blue in Fig. A1g).

$$L = AD(l_1) \vee AD(l_2) \vee ... \vee AD(l_n) \quad \text{(A1)}$$

$$\text{Edge} = L_\text{s} \setminus (L_\text{s} \ominus S) \quad \text{(A2)}$$

The results of the sensitivity analysis for the altitude in which the edge should be detected (l, L), as well as for the distances used to define near-edge and centre regions (D_1, D_2) are shown in Figs. A2 and A3.

A2 Conditional probability and odds ratios

Let a, b, c, d be the absolute frequencies in a 2×2 contingency-table as in Tab. A1 (reporting relative frequencies), with a total number of observations $n = a + b + c + d$. Then, the conditional probability of an event occurring given that AD air is present in the column, $P(\text{Event} \mid \text{AD})$, is given by Eq. A3, where $P(\text{AD})$ is the probability of an AD-column in the given location, and $P(\text{Event} \cap \text{AD})$ is the joint probability of the event and an AD-column. Odds are the ratio of the probability that an event occurs and the probability that it does not occur (Eqs. A4, A5). Their ratio is the odds ratio, OR (Eq. A6). Its natural

https://doi.org/10.5194/egusphere-2026-2350
Preprint. Discussion started: 8 May 2026

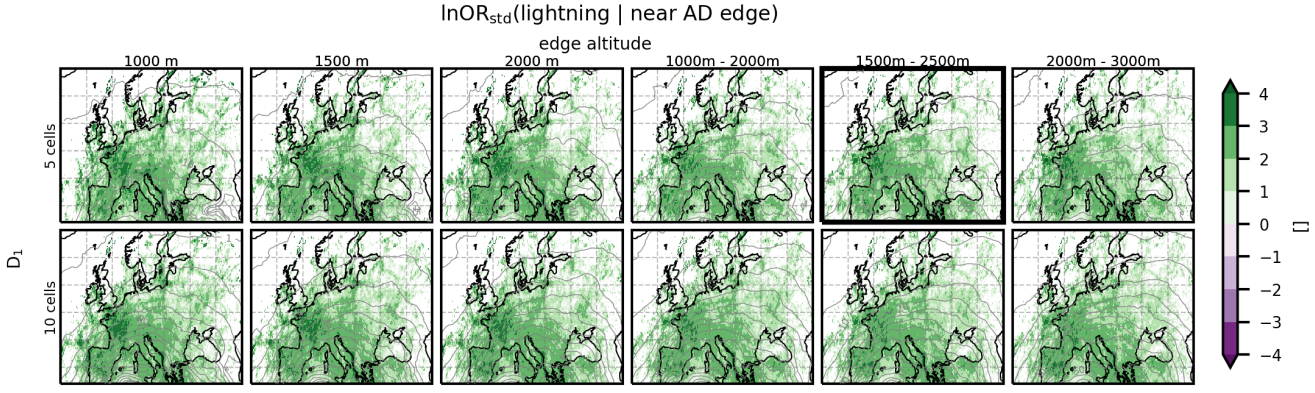

Figure A2. Standardised ln OR for lightning near AD edge, as in Fig. 3c. Columns: different altitudes for the edge detection (AD-cell centres given in the title). Rows: Different values for D_1. Subplot with thick frame is as Fig. 3c.

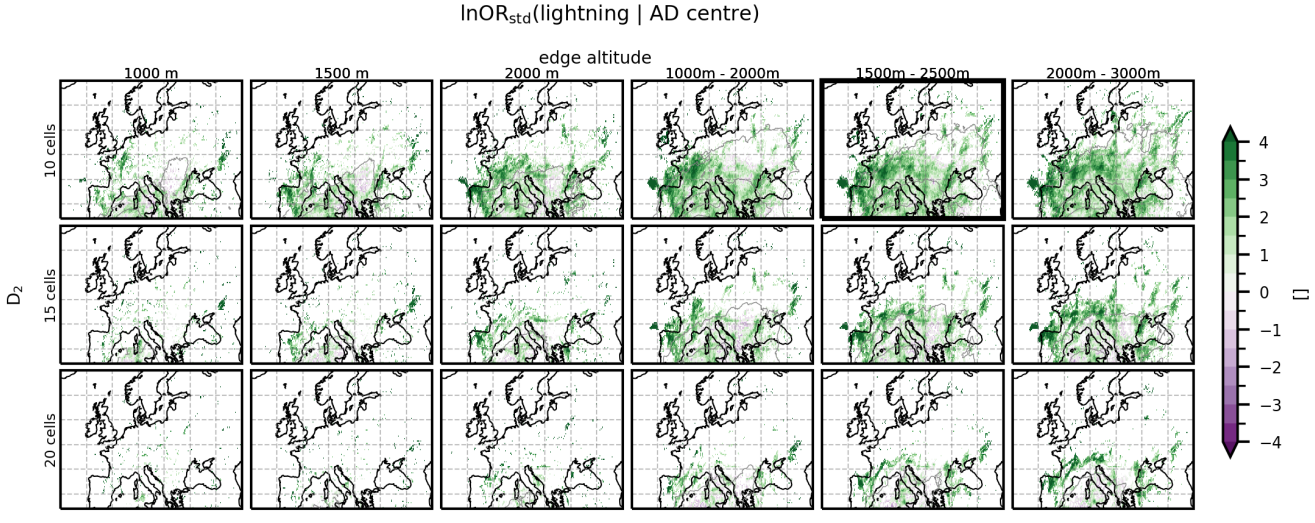

Figure A3. Standardised ln OR for lightning in AD centre, as in Fig. 3e. Columns: different altitudes for the edge detection (AD-cell centres given in the title). Rows: Different values for D_2. Subplot with thick frame is as Fig. 3e.

https://doi.org/10.5194/egusphere-2026-2350
Preprint. Discussion started: 8 May 2026

Table A1. Contingency table. n is the number of observations, a, b, c, d the absolute frequencies for the respective combination of events. 'Event' refers to an extreme weather event (e.g. strong positive temperature anomaly (PTA) or dust event). 'AD' refers to an AD-column being present.

	Event	$\overline{\text{Event}}$	
AD	$\frac{a}{n} = P(\text{AD} \cap \text{Event})$	$\frac{b}{n} = P(\text{AD} \cap \overline{\text{Event}})$	$\frac{a+b}{n} = P(\text{AD})$
$\overline{\text{AD}}$	$\frac{c}{n} = P(\overline{\text{AD}} \cap \text{Event})$	$\frac{d}{n} = P(\overline{\text{AD}} \cap \overline{\text{Event}})$	$\frac{c+d}{n} = P(\overline{\text{AD}})$
	$\frac{a+c}{n} = P(\text{Event})$	$\frac{b+d}{n} = P(\overline{\text{Event}})$	$1 = \frac{a+b+c+d}{n}$

logarithm, $\ln \text{OR} = \ln(\text{OR})$ is useful as it is centred around zero. The standard error of the log-odds ratio, $\text{SE}(\ln \text{OR})$, can be calculated according to Eq. A7 (Stephenson, 2000). Using the standardised $\ln \text{OR}$, $\ln \text{OR}_{\text{std}} = \ln \text{OR} / \text{SE}(\ln(\text{OR}))$, makes its value comparable across regions with very different marginal probabilities.

$$P(\text{Event} \mid AD) = \frac{P(\text{Event} \cap AD)}{P(AD)} = \frac{a}{a+b} \tag{A3}$$

$$\text{odds}(\text{Event} \mid \text{AD}) = P(\text{Event} \mid \text{AD}) / P(\overline{\text{Event}} \mid \text{AD}) = \frac{a}{b} \tag{A4}$$

$$\text{odds}(\text{Event} \mid \overline{\text{AD}}) = P(\text{Event} \mid \overline{\text{AD}}) / P(\overline{\text{Event}} \mid \overline{\text{AD}}) = \frac{c}{d} \tag{A5}$$

$$\text{OR} = \frac{\text{odds}(\text{Event} \mid \text{AD})}{\text{odds}(\text{Event} \mid \overline{\text{AD}})} = \frac{ad}{bc} \tag{A6}$$

$$\text{SE}(\ln(\text{OR})) = \sqrt{\frac{1}{a} + \frac{1}{b} + \frac{1}{c} + \frac{1}{d}} \tag{A7}$$

Appendix B: Supporting figures

Figure B1a shows the median of the 2m temperature given that AD air is present in the same column, while Fig. B1b shows the median given there is no AD air present. Their difference is shown in Fig. B1c. The entire domain is warmer for AD periods than for non-periods, most strikingly in western France and over the British Isles.

Figure B2 shows the properties of the cap. A cap occurs, when the lowest Ad trajectory in that cell is within the 500 m above the local BLH, and the gradient of the potential temperature over those 500 m is greater than 10 Kkm^{-1}. This differs from the definition of the lid used in Fix-Hewitt et al. (2026), which defined a lid, when the centre of the lowest AD *cell* is within $\pm$500 m of the local BLH and does not impose a stability criterion. The pattern of the probability and duration of the cap is comparable to the one shown for the lid in Fix-Hewitt et al. (2026), but the probabilities are noticeably lower and the prevalence is even shorter.

https://doi.org/10.5194/egusphere-2026-2350
Preprint. Discussion started: 8 May 2026

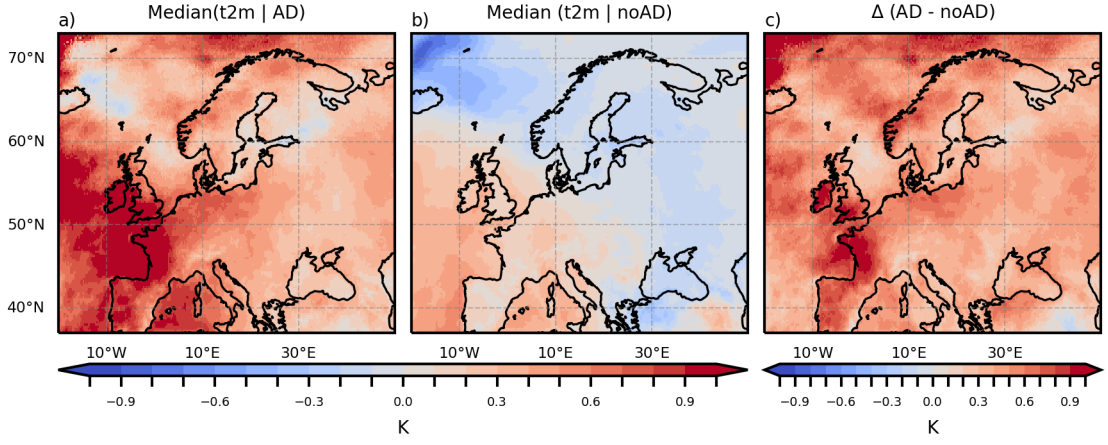

Figure B1. a) Median t2m given the presence of AD. **b)** Median t2m given the absence of AD. **c)** The difference between AD and non-AD periods.

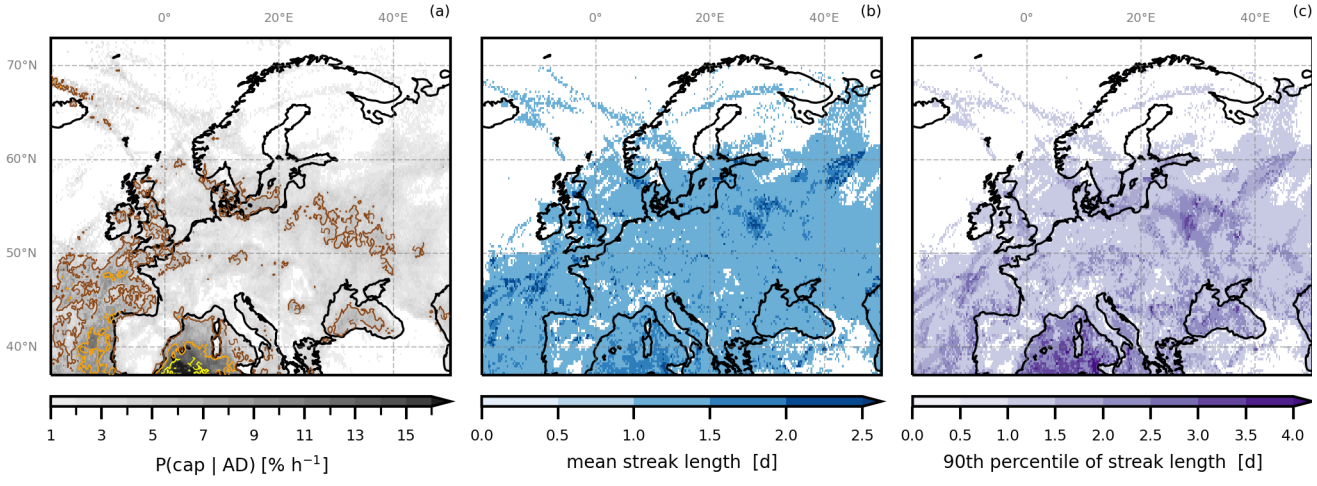

Figure B2. Cap properties. **(a)** Probability of a cap being present, given an AD is present, $P(\mathrm{Cap}|\mathrm{AD})$. The 5% (brown), 10% (orange) and 15% (yellow) contours are shown for better visibility. **(b)** Mean streak length of the cap in days. **(c)** 90th percentile of streak length of the cap in days.

https://doi.org/10.5194/egusphere-2026-2350
Preprint. Discussion started: 8 May 2026

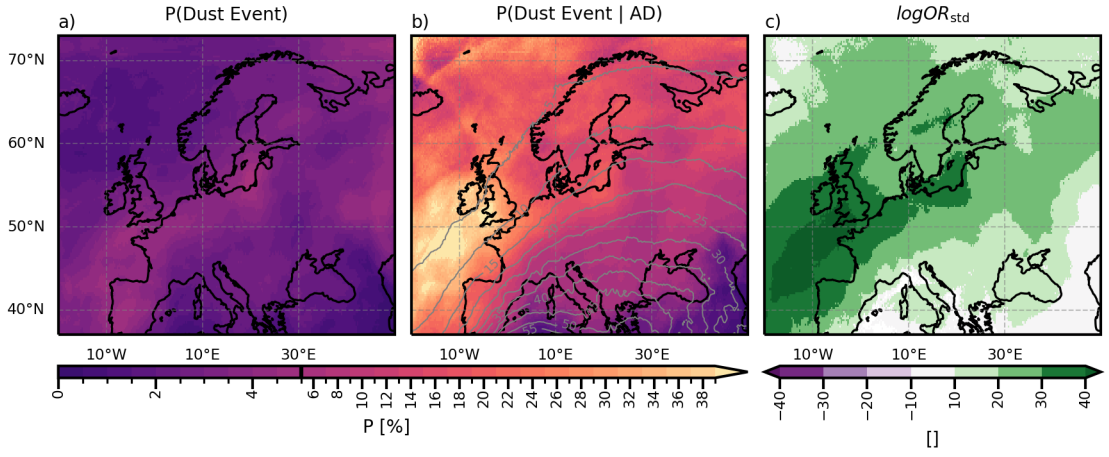

Figure C1. As Figure 5 but for extreme dust events (duaod550' > 4).

Appendix C: Extreme events

The analysis in the main body of this study was conducted for positive temperature anomaly and dust events based on an exceedance of the climatological values by 2 standard deviations ($x' > 2$, Eq. 1). Here we present results for *extreme* positive temperature anomaly and dust events, were $x' > 4$. It is striking that for dust events, the results are very similar. While the total probabilities are obviously lower for a more extreme event, the pattern and also magnitude of the standardised $\ln$OR indicate also here that ADs bring dust very frequently (compare Figs. 5c and C1c). On the other hand, the pattern is different for positive temperature anomaly events (Fig. 1) and strong positive temperature anomaly events (Fig. C2). Only over the British Isles is the signal strongly positive, indicating that for all other regions, the very strong positive temperature anomaly events are not strongly related to the presence of ADs, while the less extreme events are.

https://doi.org/10.5194/egusphere-2026-2350
Preprint. Discussion started: 8 May 2026

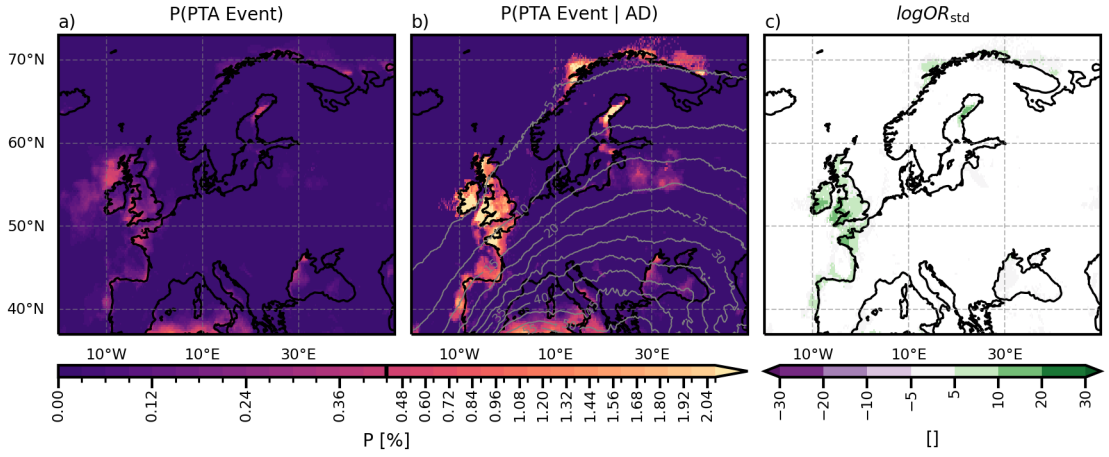

Figure C2. As Figure 1 but for extreme positive temperature anomaly events (PTA, t2m' > 4).

References

Andrews, M. S., Gensini, V. A., Haberlie, A. M., Ashley, W. S., Michaelis, A. C., and Taszarek, M.: Climatology of the Elevated Mixed Layer over the Contiguous United States and Northern Mexico Using ERA5: 1979–2021, Journal of Climate, 37, 1833–1851, https://doi.org/10.1175/JCLI-D-23-0517.1, 2024.

Arritt, R. W., Wilczak, J. M., and Young, G. S.: Observations and Numerical Modeling of an Elevated Mixed Layer, Monthly Weather Review, 120, 2869–2880, https://doi.org/10.1175/1520-0493(1992)120<2869:OANMOA>2.0.CO;2, 1992.

Banacos, P. C. and Ekster, M. L.: The Association of the Elevated Mixed Layer with Significant Severe Weather Events in the Northeastern United States, Weather and Forecasting, 25, 1082–1102, https://doi.org/10.1175/2010WAF2222363.1, 2010.

Bangert, M., Nenes, A., Vogel, B., Vogel, H., Barahona, D., Karydis, V. A., Kumar, P., Kottmeier, C., and Blahak, U.: Saharan dust event impacts on cloud formation and radiation over Western Europe, Atmospheric Chemistry and Physics, 12, 4045–4063, https://doi.org/10.5194/ACP-12-4045-2012, 2012.

Barkan, J., Alpert, P., Kutiel, H., and Kishcha, P.: Synoptics of dust transportation days from Africa toward Italy and central Europe, Journal of Geophysical Research: Atmospheres, 110, 1–14, https://doi.org/10.1029/2004JD005222, 2005.

Carlson, T. N. and Ludlam, F. H.: Conditions for the occurrence of severe local storms, Tellus, 20, 203–226, https://doi.org/10.1111/j.2153-3490.1968.tb00364.x, 1968.

Carlson, T. N., Anthes, R. A., Schwartz, M., Benjamin, S. G., and Baldwin, D. G.: Analysis and Prediction of Severe Storms Environment, Tech. rep., American Meteorological Society, Report Number AD-A94141, 1980.

Carlson, T. N., Benjamin, S. G., and Forbes, G. S.: Elevated Mixed Layers in the Regional Severe Storm Environment: Conceptual Model and Case Studies, Monthly Weather Review, 111, 1453–1473, https://doi.org/10.1175/1520-0493(1983)111<1453:EMLITR>2.0.CO;2, 1983.

Chakraborty, S., Guan, B., Waliser, D. E., da Silva, A. M., Uluatam, S., and Hess, P.: Extending the Atmospheric River Concept to Aerosols: Climate and Air Quality Impacts, Geophysical Research Letters, 48, https://doi.org/10.1029/2020GL091827, 2021.

https://doi.org/10.5194/egusphere-2026-2350
Preprint. Discussion started: 8 May 2026

Copernicus Atmosphere Monitoring Service: CAMS global atmospheric composition forecasts, https://doi.org/10.24381/04a0b097, accessed on: 02/10/2024, 2021.

Cordeira, J. M., Metz, N. D., Howarth, M. E., and Galarneau, T. J.: Multiscale upstream and in situ precursors to the elevated mixed layer and high-impact weather over the Midwest United States, Weather and Forecasting, 32, 905–923, https://doi.org/10.1175/WAF-D-16-0122.1, 2017.

Cos, P., Olmo, M., Campos, D., Marcos-Matamoros, R., Palma, L., Ángel G Muñoz, and Doblas-Reyes, F. J.: Saharan warm-air intrusions in the western Mediterranean: identification, impacts on temperature extremes, and large-scale mechanisms, Weather Clim. Dynam, 6, 609–626, https://doi.org/10.5194/wcd-6-609-2025, 2025.

Cuevas-Agulló, E., Barriopedro, D., García, R. D., Alonso-Pérez, S., González-Alemán, J. J., Werner, E., Suárez, D., Bustos, J. J., García-Castrillo, G., García, O., África Barreto, and Basart, S.: Sharp increase in Saharan dust intrusions over the western Euro-Mediterranean in February-March 2020-2022 and associated atmospheric circulation, Atmos. Chem. Phys, 24, 4083–4104, https://doi.org/10.5194/acp-24-4083-2024, 2024.

Dahl, J. M. and Fischer, J.: The origin of western European warm-season prefrontal convergence lines, Weather and Forecasting, 31, 1417–1431, https://doi.org/10.1175/WAF-D-15-0161.1, 2016.

de Villiers, M. P.: Europe extreme heat 22–26 July 2019: was it caused by subsidence or advection?, Weather, 75, 228–235, https://doi.org/10.1002/wea.3717, 2020.

Dezfuli, A., Bosilovich, M. G., and Barahona, D.: A Dusty Atmospheric River Brings Floods to the Middle East, Geophysical Research Letters, 48, https://doi.org/10.1029/2021GL095441, 2021.

England, M. H., Li, Z., Huguenin, M. F., Kiss, A. E., Gupta, A. S., Holmes, R. M., and Rahmstorf, S.: Drivers of the extreme North Atlantic marine heatwave during 2023, Nature 2025 642:8068, 642, 636–643, https://doi.org/10.1038/s41586-025-08903-5, 2025.

Enno, S. E., Sugier, J., Alber, R., and Seltzer, M.: Lightning flash density in Europe based on 10 years of ATDnet data, Atmospheric Research, 235, https://doi.org/10.1016/j.atmosres.2019.104769, 2020.

Farrell, R. J. and Carlson, T. N.: Evidence for the Role of the Lid and Underrunning in an Outbreak of Tornadic Thunderstorms, Monthly Weather Review, 117, 857–871, https://doi.org/https://doi.org/10.1175/1520-0493(1989)117<0857:EFTROT>2.0.CO;2, 1989.

Feldmann, M., Germann, U., Gabella, M., and Berne, A.: A characterisation of Alpine mesocyclone occurrence, Weather and Climate Dynamics, 2, 1225–1244, https://doi.org/10.5194/WCD-2-1225-2021, 2021.

Feldmann, M., Domeisen, D. I., and Martius, O.: A pan-European analysis of large-scale drivers of severe convective outbreaks, Weather and Climate Dynamics, 6, 1089–1106, https://doi.org/10.5194/WCD-6-1089-2025, 2025.

Fix, F., Mayr, G., Zeileis, A., Stucke, I., and Stauffer, R.: Detection and consequences of atmospheric deserts: insights from a case study, Weather Clim. Dynam, 5, 1545–1560, https://doi.org/10.5194/wcd-5-1545-2024, 2024.

Fix-Hewitt, F.: Code used in preparation of the manuscript "Atmospheric deserts and extreme weather events: co-occurrence with positive temperature anomalies, thunderstorms, and dust" by Fix-Hewitt et al., 2026, https://doi.org/10.5281/zenodo.19658813, 2026.

Fix-Hewitt, F., Zeileis, A., Stucke, I., Stauffer, R., and Mayr, G. J.: Properties and characteristics of atmospheric deserts over Europe: a first statistical analysis, Weather Clim. Dynam, 7, 17–35, https://doi.org/10.5194/wcd-7-17-2026, 2026.

Francis, D., Fonseca, R., Nelli, N., Bozkurt, D., Picard, G., and Guan, B.: Atmospheric rivers drive exceptional Saharan dust transport towards Europe, Atmospheric Research, 266, 105 959, https://doi.org/10.1016/J.ATMOSRES.2021.105959, 2022.

Garratt, J. R.: Review: the atmospheric boundary layer, Earth-Science Reviews, 37, 89–134, 1994.

https://doi.org/10.5194/egusphere-2026-2350
Preprint. Discussion started: 8 May 2026

Gkikas, A., Hatzianastassiou, N., and Mihalopoulos, N.: Aerosol events in the broader Mediterranean basin based on 7-year (2000-2007) MODIS C005 data, 27, 3509–3522, www.ann-geophys.net/27/3509/2009/, 2009.

Haralick, R. M., Sternberg, S. R., and Zhuang, X.: Image Analysis Using Mathematical Morphology, IEEE Transactions on Pattern Analysis and Machine Intelligence, PAMI-9, 532–550, https://doi.org/10.1109/TPAMI.1987.4767941, 1987.

Helmert, J., Heinold, B., Tegen, I., Hellmuth, O., and Wendisch, M.: On the direct and semidirect effects of Saharan dust over Europe: A modeling study, Journal of Geophysical Research: Atmospheres, 112, https://doi.org/10.1029/2006JD007444, 2007.

Hermes, K., Quinting, J., Grams, C. M., Hoose, C., and Hoshyaripour, G. A.: Impact of Saharan dust outbreaks on short-range weather forecast errors in Europe, Quarterly Journal of the Royal Meteorological Society, 150, 1704–1723, https://doi.org/10.1002/QJ.4666, 2024.

Hersbach, H., Bell, B., Berrisford, P., Hirahara, S., Horányi, A., Muñoz-Sabater, J., Nicolas, J., Peubey, C., Radu, R., Schepers, D., Simmons, A., Soci, C., Abdalla, S., Abellan, X., Balsamo, G., Bechtold, P., Biavati, G., Bidlot, J., Bonavita, M., Chiara, G. D., Dahlgren, P., Dee, D., Diamantakis, M., Dragani, R., Flemming, J., Forbes, R., Fuentes, M., Geer, A., Haimberger, L., Healy, S., Hogan, R. J., Hólm, E., Janisková, M., Keeley, S., Laloyaux, P., Lopez, P., Lupu, C., Radnoti, G., de Rosnay, P., Rozum, I., Vamborg, F., Villaume, S., and Thépaut, J. N.: The ERA5 global reanalysis, Quarterly Journal of the Royal Meteorological Society, 146, 1999–2049, https://doi.org/10.1002/qj.3803, 2020.

Hersbach, H., Bell, B., Berrisford, P., Biavati, G., Horányi, A., Sabater, J. M., Nicolas, J., Peubey, C., R., R., Rozum, I., Schepers, D., Simmons, A., Soci, C., Dee, D., and Thépaut, J.-N.: ERA5 hourly data on single levels from 1940 to present. Copernicus Climate Change Service (C3S) Climate Data Store (CDS), https://doi.org/10.24381/cds.adbb2d47, accessed on 18-03-2024, 2023.

Inness, A., Ades, M., Agustí-Panareda, A., Barr, J., Benedictow, A., Blechschmidt, A. M., Dominguez, J. J., Engelen, R., Eskes, H., Flemming, J., Huijnen, V., Jones, L., Kipling, Z., Massart, S., Parrington, M., Peuch, V. H., Razinger, M., Remy, S., Schulz, M., and Suttie, M.: The CAMS reanalysis of atmospheric composition, Atmospheric Chemistry and Physics, 19, 3515–3556, https://doi.org/10.5194/ACP-19-3515-2019, 2019.

Israelevich, P., Ganor, E., Alpert, P., Kishcha, P., and Stupp, A.: Predominant transport paths of Saharan dust over the Mediterranean Sea to Europe, Journal of Geophysical Research: Atmospheres, 117, 2205, https://doi.org/10.1029/2011JD016482, 2012.

Johns, R. H. and Dorr, R. A.: Some Meteorological Aspects of Strong and Violent Tornado Episodes in New England and Eastern New York, National Weather Digest, 20, 2–12, 1996.

Juza, M., de Alfonso, M., and Ángels Fernández-Mora: Coastal ocean response during the unprecedented marine heatwaves in the western Mediterranean in 2022, State of the Planet, 4-osr8, 1–11, https://doi.org/10.5194/SP-4-OSR8-14-2024, 2024.

Keyser, D. and Carlson, T. N.: Transverse Ageostrophic Circulations Associated with Elevated Mixed Layers, Monthly Weather Review, 112, 2465–2478, https://doi.org/10.1175/1520-0493(1984)112<2465:TACAWE>2.0.CO;2, 1984.

Knippertz, P.: Meteorological aspects of dust storms, Mineral Dust: A Key Player in the Earth System, pp. 121–147, https://doi.org/10.1007/978-94-017-8978-3_6, 2014.

Lanicci, J. M. and Warner, T. T.: A Synoptic Climatology of the Elevated Mixed-Layer Inversion over the Southern Great Plains in Spring. Part I: Structure, Dynamics, and Seasonal Evolution, Weather and Forecasting, 6, 181–197, https://doi.org/10.1175/1520-0434(1991)006<0181:ASCOTE>2.0.CO;2, 1991a.

Lanicci, J. M. and Warner, T. T.: A Synoptic Climatology of the Elevated Mixed-Layer Inversion over the Southern Great Plains in Spring. Part III: Relationship to Severe-Storms Climatology, Weather and Forecasting, 6, 214–226, https://doi.org/10.1175/1520-0434(1991)006<0214:ASCOTE>2.0.CO;2, 1991b.

https://doi.org/10.5194/egusphere-2026-2350
Preprint. Discussion started: 8 May 2026

Lewis, M. W. and Gray, S. L.: Categorisation of synoptic environments associated with mesoscale convective systems over the UK, Atmospheric Research, 97, 194–213, https://doi.org/10.1016/J.ATMOSRES.2010.04.001, 2010.

Li, F., Chavas, D. R., Reed, K. A., Rosenbloom, N., and Dawson, D. T.: The Role of Elevated Terrain and the Gulf of Mexico in the Production of Severe Local Storm Environments over North America, Journal of Climate, 34, 7799–7819, https://doi.org/10.1175/JCLI-D-20-0607.1, 2021.

Mohr, S., Wandel, J., Lenggenhager, S., and Martius, O.: Relationship between atmospheric blocking and warm-season thunderstorms over western and central Europe, Quarterly Journal of the Royal Meteorological Society, 145, 3040–3056, https://doi.org/10.1002/QJ.3603, 2019.

Penner, J. E., Andreae, M., Annegarn, H., Barrie, L., Feichter, J., Hegg, D., Jayaraman, A., Leaitch, R., Murphy, D., Nganga, J., Pitari, G., Ackerman, A., Adams, P., Austin, P., Boers, R., Boucher, O., Chin, M., Chuang, C., Collins, B., Cooke, W., Demott, P., Feng, Y., Fischer, H., Fung, I., Ghan, S., Ginoux, P., Gong, S.-L., Guenther, A., Herzog, M., Higurashi, A., Kaufman, Y., Kettle, A., Kiehl, J., Koch, D., Lammel, G., Land, C., Lohmann, U., Madronich, S., Mancini, E., Mishchenko, M., Nakajima, T., Quinn, P., Rasch, P., Roberts, D. L., Savoie, D., Schwartz, S., Seinfeld, J., Soden, B., Tanré, D., Taylor, K., Tegen, I., Tie, X., Vali, G., Dingenen, R. V., Weele, M. V., and Zhang, Y.: Aerosols, their Direct and Indirect Effects, pp. 289–348, Cambridge University Press, 2001.

Peyraud, L.: Analysis of the 18 July 2005 Tornadic Supercell over the Lake Geneva Region, Weather and Forecasting, 28, 1524–1551, https://doi.org/10.1175/WAF-D-13-00022.1, 2013.

Pfahl, S., Schwierz, C., Croci-Maspoli, M., Grams, C. M., and Wernli, H.: Importance of latent heat release in ascending air streams for atmospheric blocking, Nature Geoscience 2014 8:8, 8, 610–614, https://doi.org/10.1038/ngeo2487, 2015.

Prospero, J. M., Delany, A. C., Delany, A. C., and Carlson, T. N.: The Discovery of African Dust Transport to the Western Hemisphere and the Saharan Air Layer: A History, Bulletin of the American Meteorological Society, 102, E1239–E1260, https://doi.org/10.1175/BAMS-D-19-0309.1, 2021.

Ralph, F. M., Dettinger, M. C. L., Cairns, M. M., Galarneau, T. J., and Eylander, J.: Defining "Atmospheric River": How the Glossary of Meteorology Helped Resolve a Debate, Bulletin of the American Meteorological Society, 99, 837–839, https://doi.org/10.1175/BAMS-D-17-0157.1, 2018.

Ribeiro, B. Z. and Bosart, L. F.: Elevated mixed layers and associated severe thunderstorm environments in South and North America, Monthly Weather Review, 146, 3–28, https://doi.org/10.1175/MWR-D-17-0121.1, 2018.

Röthlisberger, M. and Martius, O.: Quantifying the Local Effect of Northern Hemisphere Atmospheric Blocks on the Persistence of Summer Hot and Dry Spells, Geophysical Research Letters, 46, 10 101–10 111, https://doi.org/10.1029/2019GL083745, 2019.

Röthlisberger, M. and Papritz, L.: Quantifying the physical processes leading to atmospheric hot extremes at a global scale, Nature Geoscience 2023 16:3, 16, 210–216, https://doi.org/10.1038/s41561-023-01126-1, 2023.

Schultz, D. M., Herrerías-Azcué, F., Lowe, D., Kirshbaum, D. J., and Young, M. V.: Rethinking the Spanish plume: An airstream analysis challenges the canonical conceptual model, Quarterly Journal of the Royal Meteorological Society, 151, https://doi.org/10.1002/QJ.5070, 2025a.

Schultz, D. M., Young, M. V., and Kirshbaum, D. J.: The Spanish Plume Elevated Mixed Layer: A Review of Its Use and Misuse within the Scientific Literature, Monthly Weather Review, 153, 737–761, https://doi.org/10.1175/MWR-D-24-0139.1, 2025b.

Schulzweida, U.: CDO User Guide, https://doi.org/10.5281/zenodo.10020800, 2023.

https://doi.org/10.5194/egusphere-2026-2350
Preprint. Discussion started: 8 May 2026

Seifert, A., Bachmann, V., Filipitsch, F., Förstner, J., Grams, C. M., Hoshyaripour, G. A., Quinting, J., Rohde, A., Vogel, H., Wagner, A., and Vogel, B.: Aerosol-cloud-radiation interaction during Saharan dust episodes: the dusty cirrus puzzle, Atmos. Chem. Phys, 23, 6409–6430, https://doi.org/10.5194/acp-23-6409-2023, 2023.

Sibley, A.: Thunderstorms from a Spanish Plume event on 28 June 2011, Weather, 67, 143–146, https://doi.org/10.1002/wea.1928, 2012.

Sousa, P. M., Trigo, R. M., Barriopedro, D., Soares, P. M., and Santos, J. A.: European temperature responses to blocking and ridge regional patterns, Climate Dynamics, 50, 457–477, https://doi.org/10.1007/s00382-017-3620-2, 2018.

Sprenger, M. and Wernli, H.: The LAGRANTO Lagrangian analysis tool - Version 2.0, Geoscientific Model Development, 8, 2569–2586, https://doi.org/10.5194/gmd-8-2569-2015, (data available at: https://iacweb.ethz.ch/staff/sprenger/lagranto/, last access: 21 December 2022), 2015.

Stephenson, D. B.: Use of the "Odds Ratio" for Diagnosing Forecast Skill, Weather and Forecasting, 15, 221 – 232, https://doi.org/10.1175/1520-0434(2000)015<0221:UOTORF>2.0.CO;2, 2000.

Taszarek, M., Allen, J. T., Pucik, T., Hoogewind, K. A., and Brooks, H. E.: Severe Convective Storms across Europe and the United States. Part II: ERA5 Environments Associated with Lightning, Large Hail, Severe Wind, and Tornadoes, Journal of Climate, 33, 10 263–10 286, https://doi.org/10.1175/JCLI-D-20-0346.1, 2020.

Wanke, E., Andersen, R., and Volgnandt, T.: A World-Wide Low-Cost Community-Based Time-of-Arrival Lightning Detection and Lightning Location Network (Project Description; 11 May 2014), https://www.blitzortung.org/en/cover_your_area.php, last accessed: 21 April 2026, 2014.

Wilkinson, J. M. and Neal, R.: Exploring relationships between weather patterns and observed lightning activity for Britain and Ireland, Quarterly Journal of the Royal Meteorological Society, 147, 2772–2795, https://doi.org/10.1002/qj.4099, 2021.

Young, M. V. and Grahame, N. S.: The history of UK weather forecasting: the changing role of the central guidance forecaster. Part 6: the late twentieth century: forecasting smaller-scale features, Weather, 78, 304–312, https://doi.org/10.1002/WEA.4370, 2023.

Zschenderlein, P., Fink, A. H., Pfahl, S., and Wernli, H.: Processes determining heat waves across different European climates, Quarterly Journal of the Royal Meteorological Society, 145, 2973–2989, https://doi.org/10.1002/QJ.3599, 2019.